Journal of Cerebral Blood Flow & Metabolism (2014) 34, 415–424

www.jcbfm.com

ORIGINAL ARTICLE

Aneurysmal remodeling in the circle of Willis after carotid occlusion in an experimental model

Vincent M Tutino[1,2], Max Mandelbaum[1,3], Hoon Choi[1,3,4,5], Liza C Pope[1,4], Adnan Siddiqui[1,4,6], John Kolega[1,7] and Hui Meng[1,2,3,4]

Carotid occlusions are associated with *de novo* intracranial aneurysm formation in clinical case reports, but this phenomenon is not widely studied. We performed bilateral carotid ligation ($n = 9$) in rabbits to simulate carotid occlusion, and sham surgery ($n = 3$) for control. Upon euthanasia ($n = 3$ at 5 days, $n = 6$ at 6 months post ligation, and $n = 3$ at 5 days after sham operation), vascular corrosion casts of the circle of Willis (CoW) were created. Using scanning electron microscopy, we quantified gross morphologic, macroscopic, and microscopic changes on the endocasts and compared findings with histologic data. At 5 days, CoW arteries of ligated animals increased caliber. The posterior communicating artery (PCom) increased length and tortuosity, and the ophthalmic artery (OA) origin presented preaneurysmal bulges. At 6 months, calibers were unchanged from 5 days, PComs further increased tortuosity while presenting segmental dilations, and the OA origin and basilar terminus presented preaneurysmal bulges. This exploratory study provides evidence that flow increase after carotid occlusion produces both compensatory arterial augmentation and pathologic remodeling such as tortuosity and saccular/fusiform aneurysm. Our findings may have considerable clinical implications, as these lesser-known consequences should be considered when managing patients with carotid artery disease or choosing carotid ligation as a therapeutic option.

Journal of Cerebral Blood Flow & Metabolism (2014) **34,** 415–424; doi:10.1038/jcbfm.2013.209; published online 11 December 2013

Keywords: arterial tortuosity; carotid artery disease; carotid occlusion; circle of Willis; intracranial aneurysm; vascular remodeling

INTRODUCTION

Perfusion requirements of the brain demand precise maintenance of cerebral blood flow by the basilar artery (BA) and the common carotid arteries.[1] The immediate consequences of cerebral blood flow interruption, including cerebral ischemia and stroke, are widely known.[1] Disturbances in flow often result from carotid artery occlusion caused by moderate or severe atherosclerotic carotid stenosis, which are estimated to be present in 7.5% and 3.1% of the general population, respectively.[2] Additionally, spontaneous or traumatic arterial dissections and thromboembolic events may lead to carotid occlusion.[3]

Carotid occlusion can also be artificially induced (e.g. via ligation) as a deconstructive, interventional, or surgical option for treating complex intracranial aneurysms (IAs) that are fusiform, cavernous or giant; carotid dissections, ruptures or cavernous fistulas; or skull base tumors before resection.[4–6] Furthermore, carotid ligation may be necessary after traumatic vascular injury or inadvertent damage to the artery during endoscopic sinus surgery.[7]

Carotid occlusion also has lesser-known consequences such as pathologic vascular remodeling within the circle of Willis (CoW). An increasing number of case reports have described *de novo* aneurysm formation after predominantly iatrogenic or atherosclerotic carotid occlusion, with incidences ranging from 0.7% to 20%.[8–11] Arnaout *et al*[12] recently performed a meta-analysis of a large number of *de novo* IA cases after carotid occlusion. With unilateral carotid occlusion, the majority of IAs were found contralaterally in the anterior circulation, primarily at the anterior communicating artery and the internal carotid artery (ICA),[12] whereas with bilateral carotid occlusion, the majority of IAs were found in the posterior circulation, e.g. the basilar terminus (BT).[12–15] However, anterior *de novo* aneurysms have been reported to follow bilateral ICA occlusion,[16] presumably as a result of hemodynamic forces due to flow rerouting into the external carotid arteries and their anastomotic intracranial branches including the ophthalmic artery (OA). Such aneurysm presentation has also mirrored anterior *de novo* IAs observed in Moyamoya disease,[17] which involves progressive bilateral carotid occlusion.[18]

Experimentally, we have performed unilateral and bilateral CCA ligation (BCCA-L) in rabbits and observed a drastic flow increase in the BA[19] and *de novo* IA initiation at the BT.[20–24] Aneurysm formation was shown to be a direct, maladaptive response to elevated hemodynamic stresses. This localized response was dose dependent on blood flow increase[20] and was sustained beyond the normalization of the inciting hemodynamic insult; that is, after returning wall shear stress (WSS) to baseline levels.[22]

In this exploratory study, we hypothesized that carotid occlusion causes widespread pathologic changes in the CoW that are not limited to the BT. To test this hypothesis, we adapted our existing BCCA-L rabbit model and investigated the characteristics and extent of flow-induced vascular remodeling in the entire CoW using vascular corrosion casting and scanning electron

[1]Toshiba Stroke and Vascular Research Center, University at Buffalo, Clinical and Translational Research Center, Buffalo, New York, USA; [2]Department of Biomedical Engineering, Buffalo, New York, USA; [3]Department of Mechanical & Aerospace Engineering, Buffalo, New York, USA; [4]Department of Neurosurgery, Buffalo, New York, USA; [5]Department of Neurosurgery, SUNY Upstate Medical University, Syracuse, New York, USA; [6]Department of Radiology, Buffalo, New York, USA and [7]Department of Pathology and Anatomical Sciences, University at Buffalo, State University of New York, Buffalo, New York, USA. Correspondence: Dr H Meng, Toshiba Stroke and Vascular Research Center, University at Buffalo, Clinical and Translational Research Center, 875 Ellicott Street, Buffalo, NY 14203, USA.
E-mail: huimeng@buffalo.edu
This material is based upon work supported by the National Institutes of Health under grant number (R01NS064592).
Received 15 September 2013; revised 29 October 2013; accepted 2 November 2013; published online 11 December 2013

microscopy (SEM). Results from this preliminary work could shed light on the lesser-known aspects of carotid occlusion related to potential IA formation in the CoW.

MATERIALS AND METHODS

Bilateral Common Carotid Artery Ligation

Female New Zealand white rabbits (4 to 5 kg) underwent BCCA-L surgery ($n = 9$) and sham surgery ($n = 3$) as described previously.[20,22,24] Bilateral CCA ligation dramatically increased flow through the BA and rerouted flow in the CoW.[20] Three ligated rabbits and three sham rabbits were euthanized 5 days after surgery by intravenous injection of 100 mg/kg sodium pentobarbital. The remaining BCCA-L rabbits ($n = 6$) were euthanized at 6 months in the same manner. All procedures were approved by the Institutional Animal Care and Use Committee of the State University of New York at Buffalo. The University at Buffalo Laboratory Animal Facility was certified at the highest level by the American Association for the Assessment and Accreditation of Laboratory Animal Care International and met or exceeded the guidelines of the United States Department of Agriculture. Results from this study are reported in accordance with the ARRIVE (Animals in Research: Reporting *In* Vivo Experiments) guidelines.[25]

Vascular Corrosion Casting

Vascular corrosion casting of the CoW was performed on all animals immediately after euthanasia using Batson's No. 17 Corrosion Casting Kit (Polysciences, Inc., Warrington, PA, USA), as described elsewhere.[26] After induction of anesthesia (previously described in refs. 20,22,24), the ligated CCA was accessed via a midline incision in the neck, and heparinized saline was flushed through the vasculature at 250 mm Hg for 10 minutes. After euthanasia and perfusion, approximately 10 mL of Batson's No. 17 Corrosion Cast mixture was injected into the cerebral vasculature via carotid stump. If the distal end of the ligated CCA had clotted, vascular corrosion casting was accomplished by guiding a 4- or 5-French guide catheter endovascularly from the femoral artery to the base of the vertebral artery, at which point the animal was euthanized, perfused, and injected with the casting mixture.

After injection of the casting mixture, whole specimens were kept at 4°C overnight to allow for polymerization of the mixture to occur and to mitigate heat released during the exothermic reaction. The brain, containing the vascular endocast, was excised from the skull and placed in a beaker of 20% potassium hydroxide for 2 days on a rocking platform, with intermittent changes of solution. After the brain tissue dissolved, the cast was isolated and rinsed with distilled water.

Scanning Electron Microscopy Imaging and Mosaic Image Creation

Scanning electron microscopy was used to investigate gross morphologic, macroscopic, and microscopic features of the vascular endocasts. Branching arteries were cut ~5 mm from the CoW and perforating arteries were removed. For SEM, casts were mounted on a stand with clay, electrically coupled to the stand with graphite paint, and scatter coated with molecular carbon under vacuum. The CoW was imaged at ×50, 5.0 mV with a Hitachi SU-70 scanning electron microscope (Hitachi High

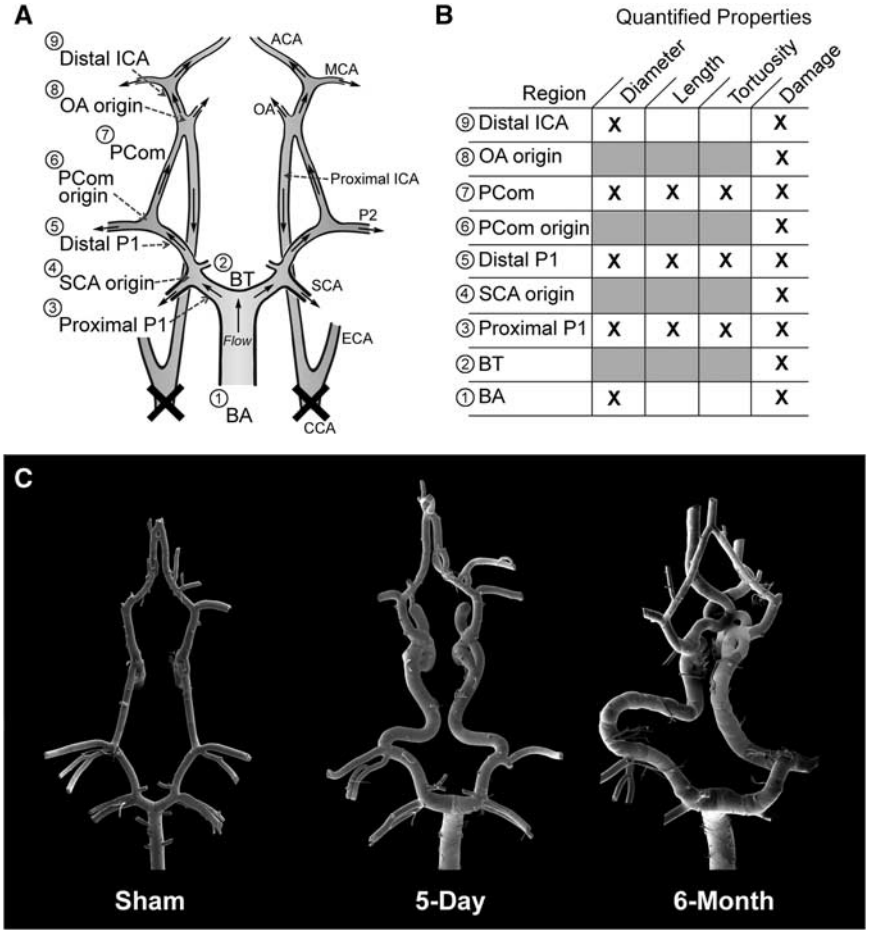

Figure 1. Overview of morphologic changes that developed in the rabbit circle of Willis (CoW) after bilateral carotid ligation. (**A**) A schematic showing flow direction after bilateral carotid ligation and nine arterial regions where damage was measured. (**B**) A chart detailing the quantified properties at each region. (**C**) Mosaic scanning electron microscopy images of vascular corrosion casts of representative CoW from the sham, 5-day, and 6-month groups. ACA, anterior cerebral artery; BA, basilar artery; BT, basilar terminus; CCA, common carotid arteries; ECA, external carotid artery; ICA, internal carotid artery; MCA, middle cerebral artery; PCom, posterior communicating artery; SCA, superior cerebellar artery.

Technologies America, Inc., Roslyn Heights, NY, USA). Areas of interest were imaged at higher magnification. Mosaic images covering the entire CoW were created at $\times 50$ using Adobe Photoshop software (Adobe Systems, Inc., San Jose, CA, USA).

Cerebral Vessel Diameter, Length, and Tortuosity Measurement

To assess the gross morphology of the CoW, diameters, and lengths of arteries were measured on mosaic images using ImageJ software (National Institutes of Health, Bethesda, MD, USA). The diameter of each vessel was recorded at three locations and averaged. The lengths of the proximal and distal P1 segments of the posterior cerebral artery (PCA) and the posterior communicating artery (PCom) were measured at the midline from the beginning to the end of each vessel segment. Only the lengths of these posterior arteries were measured, as other vessels in the CoW did not have defined beginnings or endings, thereby making length measurement impossible. Average vessel diameters and lengths were compared between each group using a Student's *t*-test ($P<0.05$).

For tortuosity quantification, we used the tortuosity index,[19] which normalizes the difference between the vessel arc length (L) and the straight-line chord distance (C) by the straight-line chord distance: $TI=(L-C)/C$. The arc and chord lengths of the proximal and distal PCA P1 segments and the PCom were measured, and tortuosity indices were calculated for each segment and averaged among each rabbit group. These average tortuosity indices were compared between each group using a Student's *t*-test ($P<0.05$). Using PCom tortuosity index data, *post hoc* power analysis in SigmaXL software (SigmaXL, Toronto, ON, Canada) revealed predicted powers of 0.99, 0.87, and 0.69 for sham versus 5-day, sham versus 6-month, and 5-day versus 6-month groups, respectively.

Quantification of Macroscopic and Microscopic Vascular Damage After Flow Increase

To quantify vascular damage throughout the CoW, we divided the mosaic SEM images into nine arterial regions comprising either branch-point regions (defined by a 500 μm radius circle about the branch apex) or connecting vessel segments. As illustrated in Figure 1A, these regions were as follows: (1) BA, (2) BT, (3) proximal PCA (proximal P1), (4) superior cerebellar artery (SCA) origin, (5) distal PCA (distal P1), (6) PCom origin, (7) PCom, (8) OA origin, and (9) distal ICA. Quantified properties measured at each location are indicated in Figure 1B.

Five types of vascular damage were observed and stratified based on the increasing severity of aneurysmal remodeling: endothelial cell (EC) irregularities—deviations from healthy, spindle-shaped, flow-aligned ECs. The presentation of a rough and irregular endothelial surface has conventionally been interpreted as a sign of EC dysfunction.[26–28] Internal elastic lamina (IEL) fenestrations—raised circular lesions on the cast surface with defined boarders, representing indentations in the vessel lumen due to focal weakening of the IEL[29] or luminal matrix degradation.[21] Smooth muscle cell (SMC) imprints—striations perpendicular to the direction of flow that are indicative of massive IEL loss, which places the endothelial layer directly onto the medial layer such that imprints of the SMC structures are visible on the cast surface.[30] These SMC imprints are distinctly different than the presentation of IEL fenestrations, which are smaller, slightly raised, and lack visible SMC structures; fenestrations indicate that the IEL is degraded but not massively, as in the case of SMC imprints. Segmental dilations—localized arterial expansions involving the entire circumference of a short vessel segment. Preaneurysmal bulges—localized outpouchings of the artery on one side of the affected vessel. This structure does not have a neck and is not a full-blown aneurysm.

The damage in each arterial region was evaluated by 3 masked observers using a progressive graded scoring method (Table 1). Our scoring system improved upon previous methods[28,31] by accounting for the presence of both macroscopic and microscopic vascular damage. This comprehensive score, termed the vascular damage score (VDS), ranged from 0 (no damage) to 30 (maximum damage). The average VDS of every region was compared between groups with a Student's *t*-test ($P<0.05$).

To determine the localization of vascular damage, the presence or absence of each type of vascular damage, regardless of degree, was analyzed at every arterial region and recorded as an occurrence frequency. The average occurrence frequency of preaneurysmal bulges and segmental dilations in every region was compared between 5-day and 6-month animals with a Student's *t*-test ($P<0.05$). Furthermore, we recorded the colocalization frequency of microscopic vascular damage to areas of macroscopic vascular damage, namely preaneurysmal bulges and segmental dilations.

Table 1. The VDS grading system accounting for five types of vascular damage

Vascular damage type	*Value*
EC Irregularities	
Low	1
Medium	2
High	3
IEL Fenestrations	
Low	4
Medium	5
High	6
SMC Imprints	
Low	7
Medium	8
High	9
Preaneurysmal bulges or segmental dilations	
Low	10
Medium	11
High	12

EC, endothelial cell; IEL, internal elastic lamina; SMC, smooth muscle cell; VDS, vascular damage score. Low, medium, and high designations refer to the extent of coverage of each type. In each of the nine arterial regions denoted in Figure 1A, individual damage types were graded, and values from all types were summed to give the VDS of that region. VDS = $\sum$(values from individual types in each arterial region).

Correlation between Vascular Tortuosity and Segmental Lesions

We examined the relationship between PCom tortuosity index and the presence of segmental dilations on the PCom. The tortuosity indices of PComs containing an equal number of segmental dilations were averaged, and the number of PCom dilations was plotted against the average tortuosity index. Power regression analysis was used to assess correlation. The average VDS for each group of PComs was also computed.

Scanning Electron Microscopy Image Comparison with Histology at the Basilar Terminus

Vascular corrosion casting prohibited any biologic investigation of vascular tissue, as all organic structures were degraded in the process of isolating the endocasts. In order to gain additional insight into structures observed on the cast surfaces, we compared our cast data with available histologic sections at the BT in rabbits that underwent BCCA-L from our previous studies.[22] We spatially matched SEM images of the endocasts at the BT with representative sections stained with van Gieson's stain for each experimental group.

RESULTS

Carotid Ligation Increased Vessel Caliber and Length at 5 days and 6 Months

Bilateral CCA ligation caused vascular remodeling in gross morphology, as shown in the representative mosaic images of vascular endocasts in Figure 1C. The vessel calibers in the 5-day BCCA-L group were significantly augment compared with sham at the BA ($54\pm9\%$, $P=0.02$), proximal P1 ($46\pm14\%$, $P=0.02$), distal P1 ($46\pm14\%$, $P=0.01$), and PCom ($74\pm5\%$, $P<0.0001$) (Figure 2A). Calibers of the 6-month BCCA-L group increased significantly at the BA ($56\pm9\%$, $P=0.001$), proximal P1 ($58\pm8\%$, $P<0.0001$), distal P1 ($49\pm6\%$, $P<0.0001$), PCom ($65\pm7\%$, $P<0.0001$), and distal ICA ($12\pm3\%$, $P=0.02$), when compared with sham (Figure 2A). However, there were no significant differences in vessel calibers between the two experimental groups.

The lengths of the proximal P1, distal P1, and PCom were measured on the endocasts. In the 5-day BCCA-L group, the length

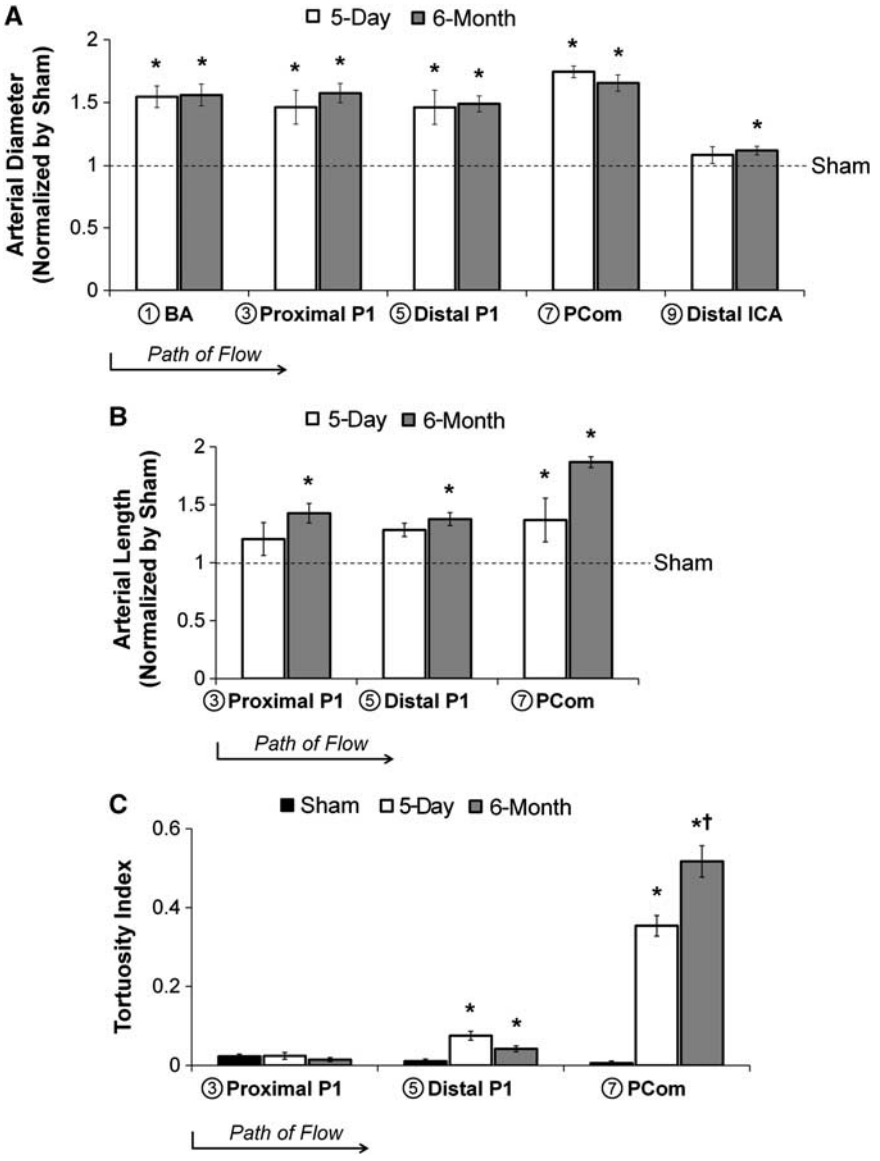

Figure 2. Arterial diameter, length, and tortuosity index at multiple locations in the circle of Willis 5 days and 6 months after bilateral carotid ligation. (**A**) Diameters of most major vessels increased significantly by 5 days and all increased significantly by 6 months. (**B**) Lengths of vessel segments in the posterior circulation increased at 5 days and 6 months. (**C**) The tortuosity index increased significantly on the distal P1 segment of the posterior cerebral artery and the posterior communicating artery. (*$P<0.05$ compared against sham. †$P<0.05$ compared against 5-day). BA, basilar artery; ICA, internal carotid artery; PCom, posterior communicating artery.

of the PCom, but not that of the proximal P1 or the distal P1, was significantly increased when compared with sham ($37 \pm 19\%$, $P = 0.03$) (Figure 2B). The proximal P1 ($43 \pm 8\%$, $P = 0.005$), distal P1 ($38 \pm 6\%$, $P = 0.004$), and the PCom ($89 \pm 5\%$, $P = 0.001$) in 6-month BCCA-L casts were significantly increased compared with those in sham casts (Figure 2B). There were no significant differences in vessel length between the two experimental groups.

Carotid Ligation Increased Tortuosity in the Posterior Communicating Artery Progressively

Vessels of the posterior circulation were more tortuous in the experimental group than in the sham group, as shown in Figure 1C. To quantify tortuosity, we used a previously described index based on the vessel arc-to-chord ratio. As shown in Figure 2C, the tortuosity index on the proximal P1 was unchanged across all groups, whereas on the distal P1, it was increased significantly in both experimental groups, compared with sham. Yet, by far, the largest increase in tortuosity index was on the PCom: 0.35 ± 0.03 for the 5-day ligated group ($P = 0.0001$) and 0.52 ± 0.04 for the 6-month ligated group ($P < 0.0001$), compared with the tortuosity index of sham (0.006 ± 0.005). Furthermore, PCom tortuosity index of the 6-month group was significantly higher compared with the 5-day group ($P = 0.004$).

Gross Aneurysmal Changes after Flow Increase

Besides vessel caliber, length and tortuosity increase, carotid ligation also resulted in aneurysmal changes within the CoW. At the macroscopic level, we observed two types of aneurysmal remodeling: bulges and segmental dilations. Overall, the most noticeable preaneurysmal bulges were found at the BT and at the OA origin, whereas most segmental dilations were found on the PCom. The presentation of these structures was as follows:

Preaneurysmal bulges. In the 5-day ligated group, 60% of the casts presented preaneurysmal bulges exclusively at the OA origin (Figures 3A and 3C). In the 6-month ligated group, these lesions presented at other branch points in the CoW. Preaneurysmal bulges varied in size, ranging from small blips to large lesions. Most distinctive were the preaneurysmal bulges that presented at the BT (50% of the casts) and the OA origin (55% of the casts) (Figures 3B and 3C). Such development was not observed in sham casts.

Segmental dilations. In the 5-day ligated group, 17% of the casts presented minor segmental dilatations on the PCom, which were observed as slight dilations around the vessel (Figures 3D and 3F). In the 6-month ligated group, 78% of the casts presented large segmental dilatations exclusively on the PCom. On average, these segmental dilatations increased vessel diameter $13 \pm 2\%$, $P = 0.04$ (Figures 3E and 3F). Such development was not observed in sham casts.

Microscopic Pathologic Changes after Flow Increase

In addition to preaneurysmal bulges and segmental dilations, damage at the microscopic level, including EC irregularities, IEL fenestrations, and SMC imprints, was also observed on the endocasts of the experimental groups. The presentation of these structures was as follows:

EC irregularities. As expected, ECs aligned parallel to the flow in straight vessel segments. Irregular EC morphology presented at the saddles of bifurcations in the 5-day and 6-month BCCA-L groups (Figure 4A). Furthermore, in the 6-month ligated group, some casts were devoid of ECs at preaneurysmal bulges, indicating the presence of an acellular environment (Figure 4B).

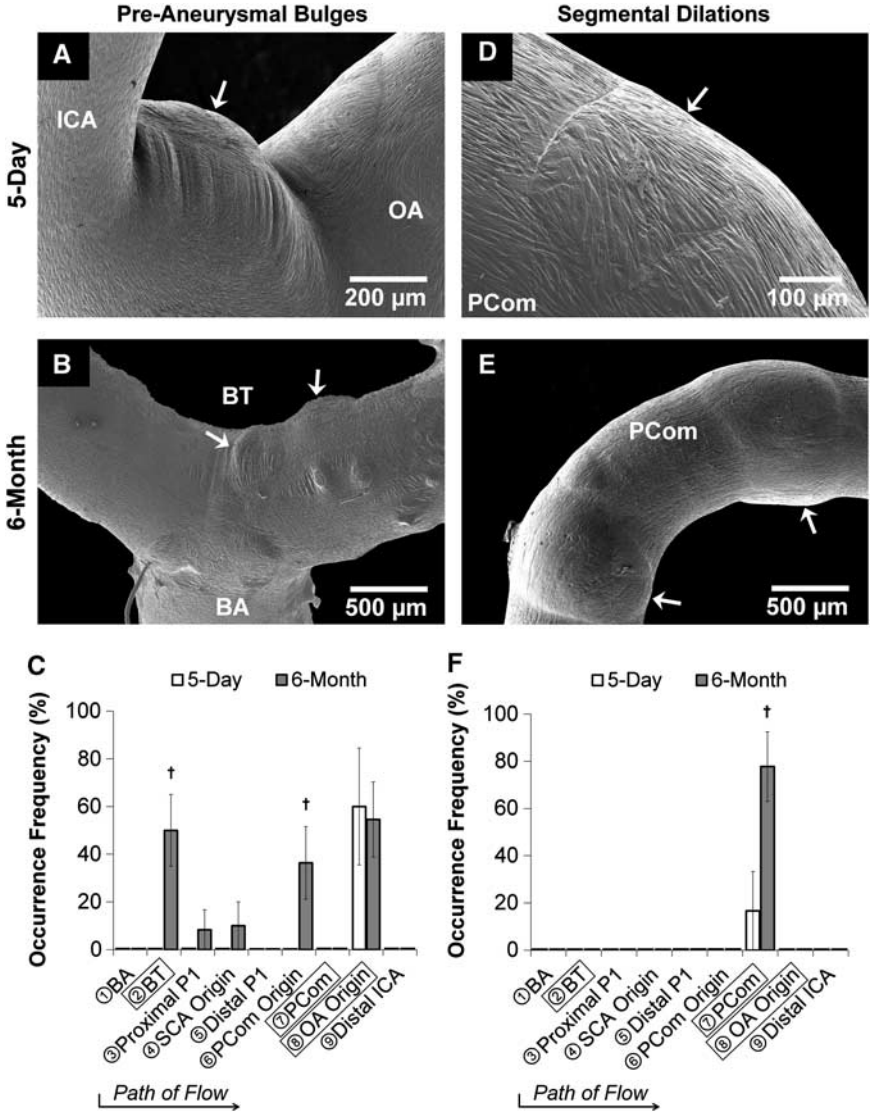

Figure 3. Gross aneurysmal remodeling in the circle of Willis after bilateral carotid ligation evident from scanning electron microscopy images of vascular casts (**A**, **B**, **D**, **E**) with occurrence frequency at each arterial region being examined (**C**, **F**). Left column (**A**–**C**): Preaneurysmal bulges. In the 5-day group, preaneurysmal bulges presented only at the ophthalmic artery (OA) origin (**A**), whereas in the 6-month group notable bulges presented at both the OA origin and the basilar terminus (**B**), with less frequent bulging at other regions (**C**). Right column (**D**–**F**): Segmental dilations. In the 5-day group, shallow segmental dilations formed on the posterior communicating artery (PCom) (**D**), whereas multiple large segmental dilations presented on the PCom at 6 months (**E**, **F**). ($^{\dagger}P < 0.05$ compared against 5-day). BA, basilar artery; BT, basilar terminus; ICA, internal carotid artery; SCA, superior cerebellar artery.

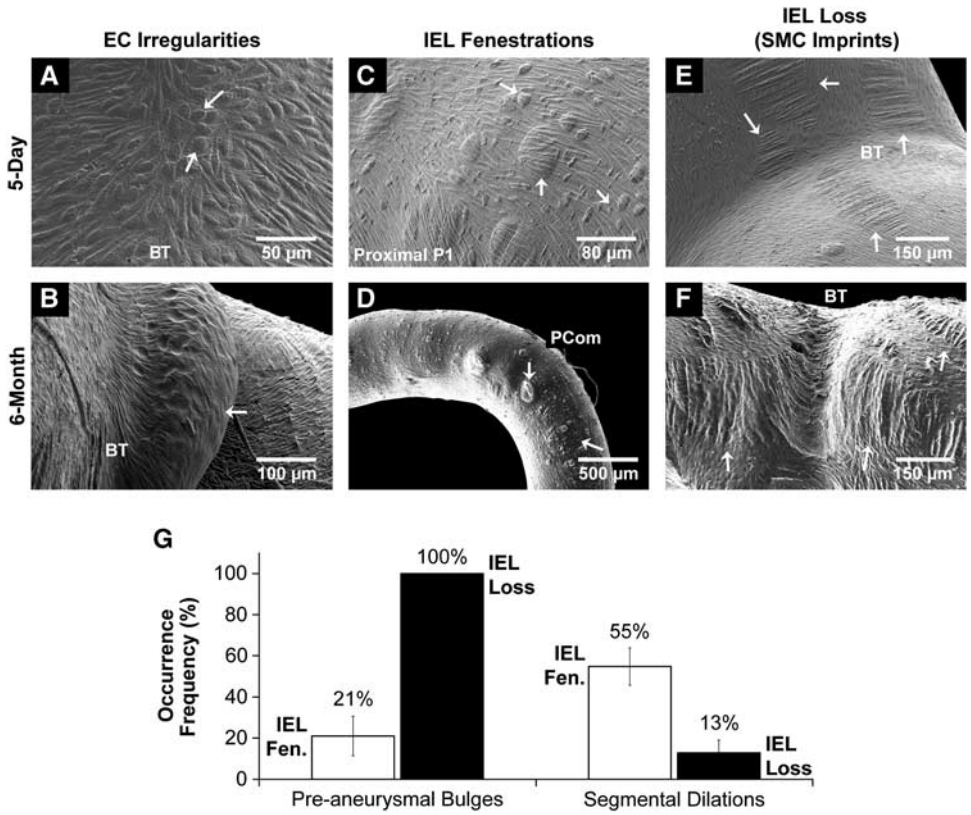

Figure 4. Microscopic changes in the circle of Willis after bilateral carotid ligation. (**A**, **B**). Endothelial cell irregularities were noted at the saddles of most bifurcations (**A**), but cell loss was observed only in the 6-month experimental group (**B**). (**C**, **D**) Internal elastic lamina (IEL) fenestrations presented in the 5-day experimental group (**C**) and more severely in the 6-month group (**D**). (**E**, **F**) Smooth muscle cell (SMC) imprints were found on both 5-day (**E**) and 6-month groups (**F**). (**G**) Correlation of gross aneurysmal remodeling with levels of IEL damage. All (100%) of preaneurysmal bulges had IEL loss, whereas only 21% of them showed IEL fenestration. However, 55% of segmental dilated regions hand IEL fenestration, whereas only 13% of them had IEL loss. BT, basilar terminus; EC, endothelial cell; PCom, posterior communicating artery.

Only sparse EC irregularities were observed in bifurcation saddles on sham casts.

IEL fenestrations. In the 5-day BCCA-L group, IEL fenestrations (Figure 4C) were present throughout the CoW. They were most densely populated on the proximal P1, distal P1, and PCom, and were less frequently present on the BT. They varied in size from 5 to 50 μm in diameter, and in some cases reached 100 μm. In the 6-month group, presentation was similar to that of the 5-day group with the exception of the PCom, where IEL fenestrations were less frequent but larger in size (Figure 4D). This structure was not observed in sham casts.

SMC imprints. In the 5-day group, there were a large amount of SMC imprints at the OA origin, the BT, the PCA, and PCom (Figure 4E). In the 6-month group, large regions of SMC imprints (IEL loss) at these regions were more numerous when compared with 5-day casts. At bifurcations, SMC imprints often existed on top of preaneurysmal bulges, and on straight vessels, they existed independently of segmental dilations (Figure 4F). This structure was not observed in sham casts.

Internal Elastic Lamina Loss Colocalizes with Preaneurysmal Bulges, whereas Internal Elastic Lamina Fenestrations Colocalize with Segmental Dilations

To investigate the possible role of IEL damage in the pathogenesis of macroscopic damage, we analyzed the localization of IEL fenestrations and SMC imprints (IEL loss) to preaneurysmal bulges and segmental dilations. All (100%) of preaneurysmal bulges were colocalized with IEL loss, whereas only few ($21 \pm 9.6\%$) had IEL fenestrations (Figure 4G). However, segmental dilations principally colocalized with regions of IEL fenestrations ($55 \pm 9.1\%$) and not SMC imprints ($13 \pm 6.1\%$) (Figure 4G). This is consistent with the widely accepted observation that IEL loss is a hallmark of saccular IA.

Vascular Damage was Progressive with Time

We used the VDS (see Table 1) to quantify vascular damage in the CoW. In the 5-day group, the VDS was significantly increased in six arterial regions: the BT, proximal P1, distal P1, PCom, and OA origin (Figure 5A). Microscopic damage contributed primarily to the increase in VDS at these regions compared with sham, except the OA origin, which developed preaneurysmal bulges. In the 6-month group, the VDS was significantly increased in all regions except the distal ICA when compared with sham (Figure 5A). When compared with the 5-day group, the 6-month group had significantly increased VDS at the BT, proximal P1, PCom origin, and PCom, primarily because of increased preaneurysmal bulges and segmental dilations.

Of the three arterial regions that had the highest VDS (the BT, PCom, and OA origin), we noticed striking differences between 5-day and 6-month groups. After the flow direction, the BT presented SMC striations at 5 days and preaneurysmal bulges at 6 months (Figures 5B1 and 5B2), the PCom was populated with IEL fenestrations at 5 days and then presented segmental dilations at 6 months (Figures 5B3 and 5B4), and the OA origin presented preaneurysmal bulges at both time points (Figures 5B5 and 5B6). These changes were reflected in the VDS at both time points.

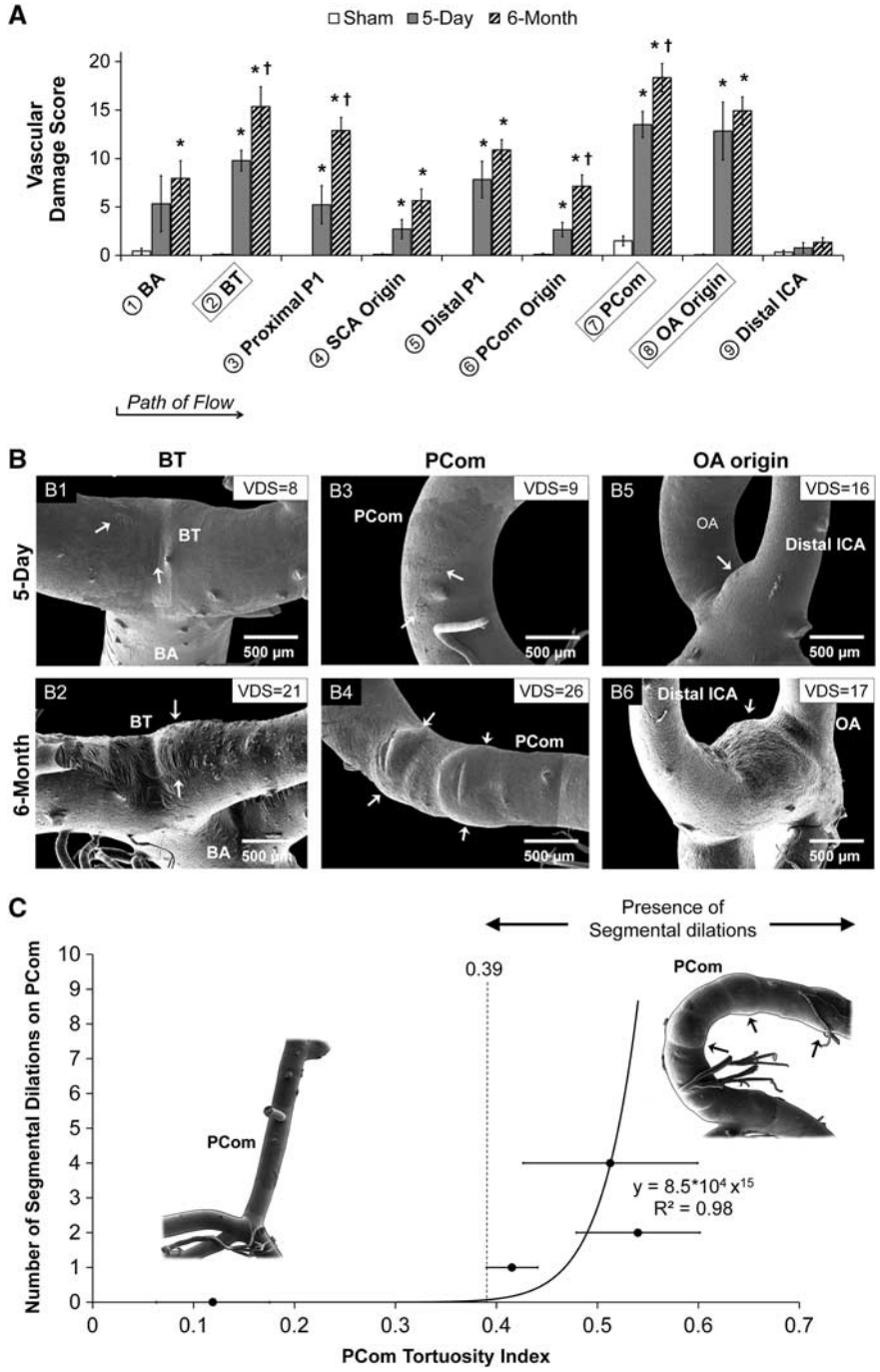

Figure 5. Quantification of aneurysmal changes in the circle of Willis (CoW) after bilateral carotid ligation. (**A**) Vascular damage score (VDS), which summates individual values accounting for different types of aneurysmal changes (as defined in Table 1) in each arterial region on the CoW of rabbits from each group, evaluated by 3 masked observers (mean ± s.e.). Damage was found throughout the CoW at 5 days and was increased at 6 months in all locations. (*$P<0.05$ compared against sham. †$P<0.05$ compared against 5-day). (**B**–**G**) Representative scanning electron microscopy images of regions with high scores: (B1) VDS = 8 owing to smooth muscle cell imprints (loss of internal elastic lamina, IEL), (B2) VDS = 21 owing to preaneurysmal bulging, (B3) VDS = 9 because of IEL fenestrations and IEL loss, (B4) VDS = 26 owing to segmental dilations, (B5 and 6) VDS are similar (16 and 17, respectively) owing to preaneurysmal bulging. (**C**) Correlation of the number of segmental dilations and tortuosity index on the posterior communicating artery (PCom). PComs were grouped by number of dilations and the average tortuosity index of each group was calculated (error bars, s.e.). A plot of the number of dilations versus average tortuosity index was fitted to a power function. As the number of dilations is quantized, a tortuosity index threshold of 0.39 is drawn, suggesting that dilations only develop on PComs that are sufficiently tortuous. BA, basilar artery; BT, basilar terminus; ICA, internal carotid artery; OA, ophthalmic artery; SCA, superior cerebellar artery.

Segmental Dilations Correlated with Elevated Tortuosity

We discovered that distinctive segmental dilations were present exclusively on PComs of the 6-month group, which also presented the highest tortuosity index. To test whether there was a correlation between tortuosity and segmental dilation presentation, we grouped PComs by the number of segmental dilations, calculated the average tortuosity index for each group, and then plotted the number of dilations against average tortuosity index.

This plot displayed a power trend with the equation $y = 8.5 \times 10^4 x^{15}$, $R^2 = 0.98$. Figure 5C demonstrates that segmental dilations were only present on PComs with tortuosity indices above 0.39. Owing to the presence of these lesions, the VDS of tortuous PComs (18.8 ± 1.1) was significantly greater than the VDS of those that were not tortuous (4.4 ± 1.6, $P < 0.0001$).

Aneurysmal Damage Observed at the Basilar Terminus Mirrored Histologic Findings

Mosaic SEM cast images at the BT were compared with representative BT histologic sections from rabbits that underwent BCCA-L. Figure 6 shows two sets of rabbit BTs (5-day and 6-month BCCA-L) with similar geometry and dimensions. We qualitatively matched the local environment around the bifurcation apex and found equivalent pathologic damage levels on the two types of data (Figure 6A): quasi-continuous IEL that was minimally disrupted in histology corresponded to small isolated IEL fenestrations on the endocasts, large segments of IEL loss corresponded to large areas of SMC imprints, and medial thinning due to SMC loss corresponded to acellular preaneurysmal bulges. Five-day BCCA-L BTs presented a central region of IEL loss surrounded by a region of uninterrupted IEL where small isolated IEL fenestrations presented (Figure 6B, left panel), whereas 6-month BCCA-L BTs presented an acellular bulge flanked by IEL loss and intermittent IEL fenestrations (Figure 6B, right panel).

DISCUSSION

Our data demonstrate that flow increase after carotid ligation elicits not only compensatory adaptive arterial enlargement in the CoW, but also pathologic remodeling such as tortuosity and aneurysm development. Five days after carotid ligation, we observed a significant increase in vessel calibers of the CoW as well as in the length and tortuosity of the PCom, and preaneurysmal bulge presentation at the OA origin. Although there was no additional increase in vessel diameters at 6 months post ligation versus 5 days, the PCom further increased in tortuosity and presented segmental dilations, and the OA origin and BT presented preaneurysmal bulges.

Adaptive and Pathologic Remodeling After Carotid Occlusion

Early compensatory caliber increase throughout the CoW at 5 days is an adaptive response of the cerebral arteries to the sustained elevation of blood flow, with the purpose of returning WSS to physiologic baselines.[1,32] Our results are consistent with previous studies using the BCCA-L model, where we showed that BA caliber increased immediately after carotid ligation whereas WSS in the BA decreased sharply and returned to baseline within 4 to 5 weeks.[20] After this WSS normalization, there was no further increase in BA diameter.[20] Thus, it is not surprising that in our experiments vessel calibers at 6 months were not further increased from those at 5 days.

In addition to adaptive vessel enlargement, we have shown that pathologic remodeling such as preaneurysmal bulges and segmental dilations also developed in response to carotid ligation. This is consistent with reports of IA initiation at the BT after both BCCA-L[20–22,24] and unilateral CCA ligation.[20,23] Specifically, Meng *et al*[22] found that the aneurysmal development at the BT continued out to 6 months, even after normalization of the inciting WSS and cessation of adaptive remodeling at 4 to 5 weeks. By comparing the 5-day and 6-month groups in the current study, we also found that the pathologic changes throughout the CoW increased with time. Thus, we speculate that the preaneurysmal bulges throughout the CoW are budding saccular IAs, whereas the segmental dilations are early fusiform IAs. We also note that these lesions show IEL degradation, a hallmark of aneurysmal damage.[21] Furthermore, preaneurysmal bulges occurred at bifurcations whereas segmental dilations occurred in nonbranching vessel segments, which is consistent with the clinical presentation of saccular and fusiform aneurysms, respectively. Interestingly, in our study, preaneurysmal bulges have massive IEL loss, whereas segmental dilations have only IEL fenestrations. This might suggest that these 2 types of aneurysmal lesions develop differently.

Besides aneurysmal development, PCom tortuosity increased with time after carotid ligation. Development of tortuosity on the

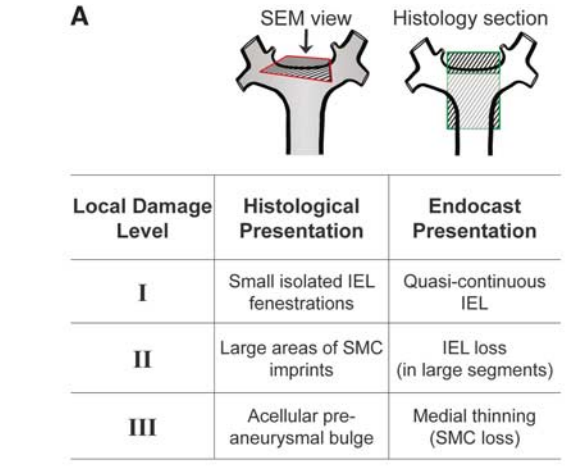

Local Damage Level	Histological Presentation	Endocast Presentation
I	Small isolated IEL fenestrations	Quasi-continuous IEL
II	Large areas of SMC imprints	IEL loss (in large segments)
III	Acellular pre-aneurysmal bulge	Medial thinning (SMC loss)

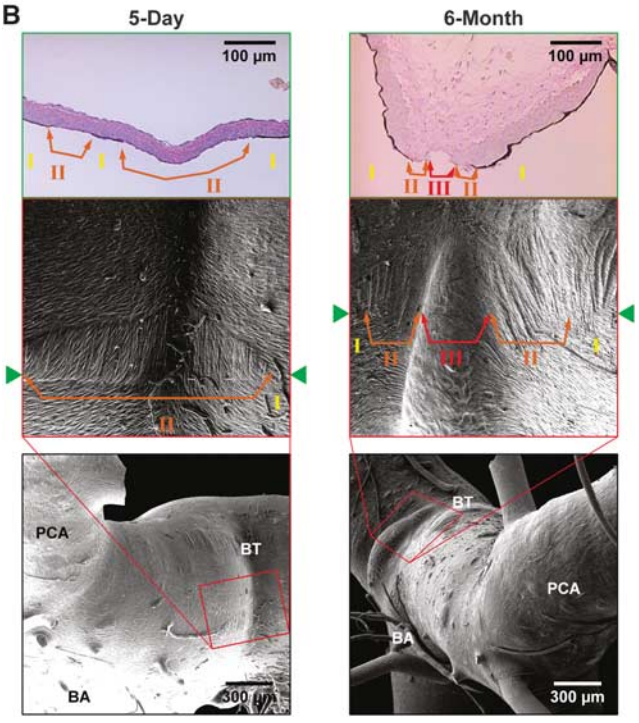

Figure 6. Comparison of aneurysmal damage presentation on scanning electron microscopy (SEM) images with presentation on histology of the basilar terminus (BT). (**A**) Correspondence of characteristics observed on endocasts and histologic sections with assignments of damage levels. (**B**) Images showing spatial correspondence of damage at equivalent levels: 5-day basilar terminus (left panel) had smooth muscle cell (SMC) imprints (loss of internal elastic lamina, IEL) flanked by isolated IEL fenestrations (quasi-continuous IEL), while 6-month BTs (right panel) had these two zones with the addition of a large acellular bulge (massive medial thinning). BA, basilar artery; PCA, posterior cerebral artery.

PCom in response to flow increase is consistent with our previous observations of tortuosity on the BA after BCCA-L.[19] The IEL fenestrations present on tortuous PComs in this study parallel focally fragmented IEL on histologic slides of tortuous BAs, suggesting that tortuosity development is facilitated by localized IEL damage.[19] (Owing to the vascular cast isolation procedure, BAs were not completely preserved; therefore, we were unable to quantify BA tortuosity in the current study)

Complex Hemodynamics in Pathological Remodeling after Carotid Occlusion

This study provides preliminary evidence that flow change subsequent to carotid ligation alone can induce pathologic remodeling and vascular damage in the CoW. Our previous studies of BT aneurysm formation in the same model (rabbit BCCA-L) have demonstrated that aneurysmal remodeling is a maladaptive response to elevated hemodynamic stresses.[22,24] Through detailed hemodynamics–histology mapping, we found that IA initiation at the BT (defined by regions of IEL loss) was associated with high WSS combined with positive WSS gradient above a threshold.[24,33] This hemodynamic condition, often associated with bifurcation apices,[34] has been recognized to independently cause *de novo* IA formation.[21,22,24,35] Kono *et al*[36] further provided clinical evidence that *de novo* BT aneurysms could be triggered by unphysiologically high local WSS and WSS gradient generated by proximal stenoses. As aneurysmal remodeling at the OA origin and the PCom in the experimental animals of the current study bears similar morphologic features to IA initiation at the BT (especially IEL damage), we postulate that flow-induced aneurysmal development at these other locations might also be induced by similar inciting hemodynamic insults. Future studies aimed at elucidating site-specific hemodynamic conditions would be required to confirm this hypothesis.

Our data also show that flow-induced segmental dilations are accompanied by progressive tortuosity increase. Although little is known about it, abnormal cerebral vascular tortuosity could be an adaptive response to increased flow burden, which manifests mechanical instability in the arterial walls.[37] In tortuous vessels, flow impinges on the outer wall of bends. To make the turn of a bend, flow along the outer curve has to travel at a higher velocity than flow along the inner curve, and has to accelerate. This creates a local hemodynamic environment with high WSS and positive WSS gradient, not dissimilar to that of bifurcation apices.[35] Based on the observed aneurysmal changes present in tortuous PComs, we speculate that high WSS and positive WSS gradient at outer curves may have triggered IEL damage[24] and aneurysmal remodeling,[19] contributing to the progressive development of tortuosity as well as segmental dilation. The relationship between tortuosity and segmental dilation and their respective etiologies should be further elucidated.

Clinical Implications

The aneurysmal development after carotid ligation in our preliminary experiments mirrors clinical case reports of *de novo* IA after carotid occlusion. Preaneurysmal bulge formation at the BT in this study may be similar to clinical cases where *de novo* aneurysms preferentially formed in the posterior circulation after bilateral carotid occlusion.[12] Likewise, the fact that the OA origin also developed preaneurysmal bulges in our study may be related to *de novo* anterior circulation IAs reported after bilateral carotid occlusion by Tasker[16] and others. We also note that preaneurysmal bulge formation observed in this study may be related to *de novo* IA formation secondary to Moyamoya disease, where aneurysms have been shown to form in both the anterior and posterior circulation (primarily the BT, peripheral vessels, anterior choroidal artery, basal ganglia branches, and ICA).[17]

Clinically, acute or chronic carotid occlusions are frequently diagnosed, sometimes with acute catastrophic consequences because of immediate flow limitation, but more commonly with few apparent effects.[38] Our study demonstrates that bilateral carotid occlusion could lead to significant pathologic remodeling, specifically aneurysm initiation and vascular tortuosity in the CoW. *De novo* IA formation and increases in cerebral vascular tortuosity are significant changes that could be detected with diagnostic angiography. The prospect of negative consequences from pathologic vascular remodeling, i.e. transient ischemic attack, stroke or subarachnoid hemorrhage, should be taken into consideration when managing patients with carotid artery occlusion, particularly when considering deconstructive approaches for cerebrovascular disease in younger patients.

Current management algorithms for carotid occlusion rely mostly on the presence of ischemic symptoms and the extent of collateral circulation.[39,40] Presently, there is no consideration for ongoing or new pathologic vascular remodeling of the neurovasculature, which could go undetected for years. Perhaps more aggressive consideration should be placed on reconstituting acute occlusion, particularly in the younger patients, as they may be exposed to a longer duration of abnormal hemodynamic insult after occlusion. In addition, routine screening and protracted follow-up vascular imaging for those with complete carotid occlusion, regardless of etiology may be warranted.

Limitations

First, we recognize that we examined only a few experimental and control replicates in this study. As no previous data was available for power analysis for these experiments, we performed *post hoc* power analysis using PCom tortuosity index data. This analysis revealed high predicted powers for comparisons between groups. Furthermore, the animals used in this study clearly answered our original question—whether there was global damage or aneurysmal remodeling throughout the CoW in response to carotid ligation. The observation of never-before-seen vascular remodeling in a majority (in some cases 100%) of the experimental groups further suggests that the number of rabbits used was sufficient for our purposes. Our quantification of morphologic changes could serve as preliminary evidence to motivate future large studies aimed at further delineating aneurysmal responses in the CoW after carotid occlusion.

Second, even though three-dimensional digital subtraction angiography was available for each animal, we did not perform computational fluid dynamics (CFD) analyses for the CoW to obtain hemodynamics at the pathologic sites. Unlike CFD modeling of a regional vascular segment that involves only one inlet (e.g. the BA) and two outlets (e.g. the PCAs), the vascular regions to be mapped in the current study would have to involve the entire CoW. In this case, CFD would be inaccurate because of multiple unknown inlet boundary conditions and especially owing to the unknown outlet velocity boundary conditions, which involve the distal vascular beds. Modeling the distal microvasculature would require many assumptions.

Third, we recognize that the flow manipulation used in this study was acute. While some carotid occlusions do occur rapidly, e.g. traumatic or iatrogenic occlusion, most of them develop over time. However, acute flow increase in the absence of other risk factors performed in this study accentuates the potential damage that hemodynamic insult could produce. When a patient harbors other risk factors and comorbidities, the resulting vascular damage could well occur even in a less acute situation, as these factors may increase susceptibility to flow-induced damage.

CONCLUSION

Although carotid occlusions have been associated with *de novo* IA formation in clinical case reports, the phenomenon has not been

widely studied. Using a carotid ligation model, this exploratory study demonstrated that compensatory cerebral blood flow increase after carotid occlusion can cause not only adaptive arterial enlargement, but also pathologic remodeling such as tortuosity and saccular/fusiform aneurysm development throughout the CoW. Our preliminary findings may have considerable clinical implications, as these lesser-known consequences of carotid occlusion/ligation should be considered when managing patients with carotid artery diseases or choosing carotid ligation as a therapeutic option.

DISCLOSURE/CONFLICT OF INTEREST

VMT—None. MM—None. HC—None. LCP—None. AS—Co-investigator of the National Institutes of Health grant (R01NS064592). Financial interests in Hotspur, Intratech Medical, StimSox, and Valor Medical. Consultant/advisory roles for Codman & Shurtleff, Concentric Medical, ev3/Covidien Vascular Therapies, GuidePoint Global Consulting, and Penumbra. Received honoraria from Abbott Vascular, Codman & Shurtleff, Genentech, and Neocure Group LLC. JK—Co-investigator of the National Institutes of Health grant (R01NS064592). HM—Principal investigator of the National Institutes of Health grant (R01NS064592).

ACKNOWLEDGMENTS

This material is based upon work supported by the National Institutes of Health under grant number (R01NS064592) (HM). We gratefully acknowledge Peter Bush for SEM instrumentation assistance, Akira Takahashi at Tohoku University for guidance on corrosion casting, and Christopher Martensen, Jessica Utzig, and Kaitlynn Olczak for help with mosaic SEM image grading.

REFERENCES

1 Paulson OB, Strandgaard S, Edvinsson L. Cerebral autoregulation. *Cerebrovasc Brain Metab Rev* 1990; **2**: 161–192.
2 de Weerd M, Greving JP, Hedblad B, Lorenz MW, Mathiesen EB, O'Leary DH *et al.* Prevalence of asymptomatic carotid artery stenosis in the general population: an individual participant data meta-analysis. *Stroke* 2010; **41**: 1294–1297.
3 Thanvi B, Robinson T. Complete occlusion of extracranial internal carotid artery: clinical features, pathophysiology, diagnosis and management. *Postgrad Med J* 2007; **83**: 95–99.
4 Gonzalez CF, Moret J. Balloon occlusion of the carotid-artery prior to surgery for neck tumors. *Am J Neuroradiol* 1990; **11**: 649–652.
5 Graves VB, Perl J, Strother CM, Wallace RC, Kesava PP, Masaryk TJ. Endovascular occlusion of the carotid or vertebral artery with temporary proximal flow arrest and microcoils: clinical results. *Am J Neuroradiol* 1997; **18**: 1201–1206.
6 Hoh B. Therapeutic internal carotid artery occlusion. In: Nussbaum ES, Mocco J eds. *Cerebral Revascularization: Microsurgical And Endovascular Techniques*. Thieme Medical Publishers, Inc.: New York, NY, 2011 147–152.
7 Fu M, Patel T, Baehring JM, Bulsara KR. Cavernous carotid pseudoaneurysm following transsphenoidal surgery. *J Neuroimaging* 2012; **23**: 319–325.
8 Briganti F, Cirillo S, Caranci F, Esposito F, Maiuri F. Development of '*de novo*' aneurysms following endovascular procedures. *Neuroradiology* 2002; **44**: 604–609.
9 Timperman PE, Tomsick TA, Tew JM, Vanloveren HR. Aneurysm formation after carotid occlusion. *Am J Neuroradiol* 1995; **16**: 329–331.
10 Fujiwara S, Fujii K, Fukui M. *De novo* aneurysm formation and aneurysm growth following therapeutic carotid occlusion for intracranial internal carotid artery (ICA) aneurysms. *Acta Neurochir (Wien)* 1993; **120**: 20–25.
11 Suzuki MT, Aguiar GB, Jory M, Conti ML, Veiga JC. *De novo* basilar tip aneurysm. Case report and literature review. *Neurocirugia (Astur)* 2011; **22**: 251–254.
12 Arnaout OM, Rahme RJ, Aoun SG, Daou MR, Batjer HH, Bendok BR. *De novo* large fusiform posterior circulation intracranial aneurysm presenting with subarachnoid hemorrhage 7 years after therapeutic internal carotid artery occlusion: case report and review of the literature. *Neurosurgery* 2012; **71**: E764–E771.
13 Lai SL, Chen YC, Weng HH, Chen ST, Hsu SP, Lee TH. Bilateral common carotid artery occlusion—a case report and literature review. *J Neurol Sci* 2005; **238**: 101–104.
14 Meguro T, Tanabe T, Muraoka K, Terada K, Rotsune N, Nishino S. Endovascular treatment of aneurysmal subarachnoid hemorrhage associated with bilateral common carotid artery occlusion. *Interv Neuroradiol* 2008; **14**: 447–452.
15 Xu K, Wang HL, Luo Q, Li Y, Yu JL. Endovascular treatment of bilateral carotid artery occlusion with concurrent basilar apex aneurysm: a case report and literature review. *Int J Med Sci* 2011; **8**: 263–269.
16 Tasker RR. Ruptured berry aneurysm of the anterior ethmoidal artery associated with bilateral spontaneous internal carotid artery occlusion in the neck. Case report. *J Neurosurg* 1983; **59**: 687–691.
17 Nagamine Y, Takahashi S, Sonobe M. Multiple intracranial aneurysms associated with moyamoya disease. Case report. *J Neurosurg* 1981; **54**: 673–676.
18 Kodama N, Sato M, Sasaki T. Treatment of ruptured cerebral aneurysm in moyamoya disease. *Surg Neurol* 1996; **46**: 62–66.
19 Hoi YM, Gao L, Tremmel M, Paluch RA, Siddiqui AH, Meng H *et al. In vivo* assessment of rapid cerebrovascular morphological adaptation following acute blood flow increase laboratory investigation. *J Neurosurg* 2008; **109**: 1141–1147.
20 Gao L, Hoi Y, Swartz DD, Kolega J, Siddiqui A, Meng H. Nascent aneurysm formation at the basilar terminus induced by hemodynamics. *Stroke* 2008; **39**: 2085–2090.
21 Kolega J, Gao L, Mandelbaum M, Mocco J, Siddiqui AH, Natarajan SK *et al.* Cellular and molecular responses of the basilar terminus to hemodynamics during intracranial aneurysm initiation in a rabbit model. *J Vasc Res* 2011; **48**: 429–442.
22 Meng H, Metaxa E, Gao L, Liaw N, Natarajan SK, Swartz DD *et al.* Progressive aneurysm development following hemodynamic insult. *J Neurosurg* 2011; **114**: 1095–1103.
23 Meng H, Natarajan SK, Gao L, Ionita C, Kolega J, Siddiqui AH *et al.* Aneurysmal changes at the basilar terminus in the rabbit elastase aneurysm model. *AJNR Am J Neuroradiol* 2010; **31**: E35–E36author reply E37.
24 Metaxa E, Tremmel M, Natarajan SK, Xiang J, Paluch RA, Mandelbaum M *et al.* Characterization of critical hemodynamics contributing to aneurysmal remodeling at the basilar terminus in a rabbit model. *Stroke* 2010; **41**: 1774–1782.
25 Kilkenny C, Browne WJ, Cuthill IC, Emerson M, Altman DG. Improving bioscience research reporting: the ARRIVE guidelines for reporting animal research. *PLoS Biol* 2010; **8**: e1000412.
26 Jamous MA, Nagahiro S, Kitazato KT, Satoh K, Satomi J. Vascular corrosion casts mirroring early morphological changes that lead to the formation of saccular cerebral aneurysm: an experimental study in rats. *J Neurosurg* 2005; **102**: 532–535.
27 Masuda H, Kawamura K, Nanjo H, Sho E, Komatsu M, Sugiyama T *et al.* Ultrastructure of endothelial cells under flow alteration. *Microsc Res Tech* 2003; **60**: 2–12.
28 Eldawoody H, Shimizu H, Kimura N, Saito A, Nakayama T, Takahashi A *et al.* Simplified experimental cerebral aneurysm model in rats: comprehensive evaluation of induced aneurysms and arterial changes in the circle of willis. *Brain Res* 2009; **1300**: 159–168.
29 Campbell GJ, Eng P, Roach MR. Fenestrations in the internal elastic lamina at bifurcations of human cerebral arteries. *Stroke* 1981; **12**: 489–496.
30 Masuda H, Zhuang YJ, Singh TM, Kawamura K, Murakami M, Zarins CK *et al.* Adaptive remodeling of internal elastic lamina and endothelial lining during flow-induced arterial enlargement. *Arterioscler Thromb Vasc Biol* 1999; **19**: 2298–2307.
31 Jamous MA, Nagahiro S, Kitazato KT, Tamura T, Kuwayama K, Satoh K. Role of estrogen deficiency in the formation and progression of cerebral aneurysms. Part ii: experimental study of the effects of hormone replacement therapy in rats. *J Neurosurg* 2005; **103**: 1052–1057.
32 Wagenseil JE, Mecham RP. Vascular extracellular matrix and arterial mechanics. *Physiol Rev* 2009; **89**: 957–989.
33 Tremmel M, Xiang J, Hoi Y, Kolega J, Siddiqui AH, Mocco J *et al.* Mapping vascular response to *in vivo* hemodynamics: application to increased flow at the basilar terminus. *Biomech Model Mechanobiol* 2010; **9**: 421–434.
34 Alfano JM, Kolega J, Natarajan SK, Xiang J, Paluch RA, Levy EI *et al.* Intracranial aneurysms occur more frequently at bifurcation sites that typically experience higher hemodynamic stresses. *Neurosurgery* 2013; **73**: 497–505.
35 Dolan JM, Kolega J, Meng H. High wall shear stress and spatial gradients in vascular pathology: a review. *Ann Biomed Eng* 2012; **41**: 1411–1427.
36 Kono K, Masuo O, Nakao N, Meng H. *De novo* cerebral aneurysm formation associated with proximal stenosis. *Neurosurgery* 2013 (e-pub ahead of print).
37 Han HC. Twisted blood vessels: symptoms, etiology and biomechanical mechanisms. *J Vasc Res* 2012; **49**: 185–197.
38 Brott TG, Halperin JL, Abbara S, Bacharach JM, Barr JD, Bush RL *et al.* 2011ASA/ACCF/AHA/AANN/AANS/ACR/ASNR/CNS/SAIP/SCAI/SIR/SNIS/SVM/SVS guideline on the management of patients with extracranial carotid and vertebral artery disease. *Stroke* 2011; **42**: e464–e540.
39 Featherstone RL, Brown MM, Coward LJ. International carotid stenting study: protocol for a randomised clinical trial comparing carotid stenting with endarterectomy in symptomatic carotid artery stenosis. *Cerebrovasc Dis* 2004; **18**: 69–74.
40 Mantese VA, Timaran CH, Chiu D, Begg RJ, Brott TG. The carotid revascularization endarterectomy versus stenting trial (crest): stenting versus carotid endarterectomy for carotid disease. *Stroke* 2010; **41**: S31–S34.